Atmos. Chem. Phys. Discuss., 13, 14545–14579, 2013
www.atmos-chem-phys-discuss.net/13/14545/2013/
doi:10.5194/acpd-13-14545-2013


Atmospheric Chemistry and Physics Discussions
Open Access



# Estimation of nocturnal $^{222}$Rn soil fluxes over Russia from TROICA measurements

**E. V. Berezina[1], N. F. Elansky[1], K. B. Moiseenko[1], I. B. Belikov[1], R. A. Shumsky[1], A. N. Safronov[1], and C. A. M. Brenninkmeijer[2]**

[1]A.M. Obukhov Institute of Atmospheric Physics, Russian Academy of Sciences, Moscow, Russia
[2]Max-Planck-Institut für Chemie, Air Chemistry Division, Mainz, Germany

Received: 13 May 2013 – Accepted: 16 May 2013 – Published: 4 June 2013

Correspondence to: E. V. Berezina (e_berezina_83@mail.ru), K. B. Moeseyenko (konst.dvina@gmail.com), and N. F. Elansky (n.f.elansky@mail.ru)

Published by Copernicus Publications on behalf of the European Geosciences Union.

## Abstract

In TROICA (TRanscontinental Observations Into the Chemistry of the Atmosphere) experiments (1999–2008) simultaneous observations of near surface $^{222}$Rn concentrations and atmospheric boundary layer thermal structure were performed across North Eurasia including the central part of Russia, South Siberia and the Far East. The data on $^{222}$Rn and temperature vertical distribution are used to estimate regional scale $^{222}$Rn soil fluxes basing on calculations of nocturnal $^{222}$Rn accumulation rates in the surface layer under inversion conditions. An effect of seasonal soil thawing on 2–4 times surface $^{222}$Rn concentration increase from summer 1999 to autumn 2005 is observed. The $^{222}$Rn flux estimated from our experiments varies over Russia from 0.01 to 0.15 Bq m$^{-2}$ s$^{-1}$ with the highest $^{222}$Rn fluxes being derived in the mountain regions of South Siberia and the Far East.


## 1 Introduction

The radioactive gas radon ($^{222}$Rn) is one of the decay products of uranium-238 ($^{238}$U), the most abundant uranium isotope in the Earth's crust. The main source of $^{222}$Rn in the atmosphere is the soil and its flux depends on the soil type and properties; its only sink is radioactive decay. $^{222}$Rn is a chemically inert gas with the half-life of 3.82 days. These features allow $^{222}$Rn to be a useful tracer to study air transport (Prospero et al., 1970; Wilkniss et al., 1974, Dörr et al., 1983; Lee and Larsen, 1997) as well as to derive emissions of some atmospheric gases: $CH_4$ and $CO_2$ (Dörr et al., 1983; Gaudry et al., 1990, Levin et al., 1999; Moriizumi et al., 1996; Schmidt et al., 1996; Duenas et al., 1999; Biraud at al., 2000; Hirsch, 2007), $N_2O$ (Biraud at al., 2000; Conen et al., 2002; Messager et al., 2008; Corazza et al., 2011), CO (Messager et al., 2008), $H_2$ (Yver et al., 2009). $^{222}$Rn is also commonly used for validating transport in climate models (Rasch, 2000; Szegvary et al., 2007), with $^{222}$Rn flux being generally assumed to be spatially uniform with a rate of 1 atom cm$^{-2}$ s$^{-1}$ (0.021 Bq m$^{-2}$ s$^{-1}$) from ice-free land surfaces and zero from oceans (Conen and Robertson, 2002). However, $^{222}$Rn flux varies widely in space and in time. Therefore, the information about spatial and temporal $^{222}$Rn flux variations over a variety of conditions is very important for correct estimation of spatial distribution and strength of natural and anthropogenic sources and sinks of greenhouse gases based on the observations of their near-surface concentrations.

$^{222}$Rn flux measurements were carried out in different regions of the world (Duenas et al., 1999; Turekian et al., 1977; Somashekarappa et al., 1996; Szegvary et al., 2007; Taguchi et al., 2011) including Russia (Milin et al., 1967; Kirichenko, 1970; Yakovleva, 2003; Tarasov, 2008). However, the data reported for Russia are not sufficient to form a clear picture of $^{222}$Rn flux variations over such a vast territory.

During the last fifteen years the substantial data on $^{222}$Rn spatial variability has been obtained with the use of a mobile carriage laboratory during international TROICA (TRanscontinental Observations Into the Chemistry of the Atmosphere) experiments along the Trans-Siberian Railroad from Moscow to Vladivistok (Elansky et al., 2009). These observations allow studying the large scale variability of near-surface atmospheric composition across extensive areas of the continent with essentially different geological, geographical and climatic features.

Preliminary results of $^{222}$Rn flux estimation from TROICA experiments are given in Berezina and Elansky (2009) (hereafter BE09). The method used in BE09 to calculate $^{222}$Rn soil flux implies a uniform vertical $^{222}$Rn distribution in a stable 100 m height surface layer based on the observations of $^{222}$Rn vertical distribution in stable atmospheric conditions presented in some investigations (Jacobi and Andre, 1963; Servant, 1966; Kataoka et al., 1998). Although such a simplification seems to be physically reasonable when studying particular events, it could lead to significant and poorly controlled errors in $^{222}$Rn emission calculations when considering such a long-distance route with strongly variable conditions affecting $^{222}$Rn fluxes.

In this paper we present a more elaborate procedure to assess regional-scale $^{222}$Rn fluxes based on simultaneous observations of surface $^{222}$Rn and temperature vertical





ACPD
13, 14545–14579, 2013

distribution in the atmospheric boundary layer (ABL) during six TROICA experiments in 1999–2008. The observational data along with the description of a simple numerical procedure to calculate vertical $^{222}$Rn distribution within the nocturnal stable ABL are presented in Sect. 2. The observed regional-scale surface $^{222}$Rn variability and derived $^{222}$Rn fluxes are discussed in Sect. 3. Finally, the general conclusions on the results of this study are formulated in Sect. 4.

## 2 Data and methodology

The TROICA observational experiments have been carried out on a regularly basis since 1995 (Elansky et al., 2009) (Table 1). In this study we use the data from six experiments in which the simultaneous measurements of $^{222}$Rn and vertical temperature profiles in ABL were performed. The complete description of the measurement technique, data quality assessment and the dataset obtained from the measurements from the railroad mobile laboratory are presented in Elansky et al. (2009).

The route of the TROICA experiments overlaid on the radon risk map of Russia (Maximovsky et. al., 1996) (see discussion below in Sect. 3.1.1) is shown in Fig. 1. The total length of the route from Moscow to Vladivostok (9288 km) is covered for approximately 6 days, so the total duration of a single campaign (forward and return paths) is about two weeks. The strength of $^{222}$Rn natural sources varies strongly along the route due to essentially different geological settings over the territory crossed by the railway. The significant part of the route is located in the mountain areas of the Southern Urals and Southern Siberia (Central and Eastern Siberia) where the $^{222}$Rn surface fluxes is known to be elevated (see Fig. 1). As the railway goes along the most densely populated and industrial regions of the European part of Russia and Southern Siberia, an anthropogenic origin of the measured $^{222}$Rn concentrations can also be important at some parts of the Trans-Siberian Railroad such as the central region of European Russia and the Southern Urals. We expect, however, that the relative effect of this signal is substantially diminished when inverting the radon flux values since the





ACPD
13, 14545–14579, 2013

most of the data in each radon accumulation event is obtained either upwind of possible anthropogenic sources or in low wind synoptic conditions, so the characteristic time of advection from such sources is comparable with the $^{222}$Rn life time.

### 2.1 $^{222}$Rn measurement technique

Surface $^{222}$Rn concentration was measured by the analyzer of $^{222}$Rn decay products LLRDM (Low Level Radon Daughters Measurement) produced by Tracer Lab (Germany). The air intake of the instrument is placed at the front side of the carriage roof at a 4 m height a.g.l. The measurement method is to determine $^{222}$Rn gas concentration via its short-lived aerosol-attached daughter activity ($^{218}$Po, $t_{1/2}$ = 3.05 min; $^{214}$Pb, $t_{1/2}$ = 26.8 min; $^{214}$Bi, $t_{1/2}$ = 19.7 min) (Martz et al., 1969; Stockburger and Sittkus, 1966) collected the moving a quartz fiber filter ribbon of the instrument. A special technique for the measurement data correction is implemented when any deviation from the radioactive equilibrium occurs. The measurement range of the instrument is 0.1–100 Bq m$^{-3}$. The data were archived as 10 min averages with an absolute measurement error to be about 15 %.

### 2.2 Temperature profiles measurements

Vertical temperature profiles were measured with the use of the MTP-5 microwave temperature profiler (ATTEX, Russia) from the level of the carriage roof (4 m a.g.l.) up to the 600 m height (the in-situ outdoor temperature measurements at 4 m a.g.l. were also conducted independently by standard meteorological thermometer). The MTP-5 measures the atmospheric thermal radiation in the center of the molecular-oxygen absorption band at around 56 GHz at different zenith angles. The brightness temperature is then retrieved from the measurements (Kadygrov and Pick, 1998) to obtain a vertical temperature profile in a range 0–600 m a.g.l. with 50 m vertical resolution. To minimize the effect of the electric locomotive and the short-term influence of different objects located near the railway on the instrument operation, zenith angle scanning was carried out at a 10° angle relative to the direction of the motion. The resolution of the retrieved temperature data is 5 min and the overall instrument accuracy is about 0.2 °C. Some relevant parameters of the observed near-surface inversions (outside the large towns and their suburbs) are summarized in Tables 2 and 4.

## 2.3 Theoretical considerations

In present study we use a simple numerical procedure to calculate $^{222}$Rn accumulation rates in the stable nocturnal ABL for a number of specific accumulation events observed during the TROICA observations. For each event, we define $t_1$ – the time of the beginning of surface inversion formation and $t_2$ – the time of the observed maximum $^{222}$Rn concentration, with the latter corresponding commonly to the time when the inversion starts to collapse. The time of a particular event varies from 3 to 13 h. Since the typical movement velocity of the mobile laboratory amounts to 50–70 km h$^{-1}$, a characteristic spatial scale $L$ for an individual event is within the range of 150–1000 km. Further, it seems to be appropriate to use the following major assumptions:

1. During each event $^{222}$Rn surface flux can be set to some constant value representing space and time averaged $^{222}$Rn emission rate over $L$;

2. Since the most part of the radon daughters are attached to submicron particles having a settling velocity less than 1 m h$^{-1}$, radon removal due to sedimentation can be neglected;

3. At the time of inversion onset $t_1$ the surface $^{222}$Rn concentration field is assumed to be spatially homogeneous over $L$;

4. Radon vertical transport due to diffusion is limited by the height of the inversion layer;

5. Any changes in local $^{222}$Rn concentrations in the near-surface layer below the inversion due to wind advection can be neglected compared to its vertical transport by eddy diffusivity.

The latter assumption is substantiated by the fact that during the observed strong surface temperature inversions horizontal air movement in ABL is generally very weak, so we do not consider air advection from any particular anthropogenic $^{222}$Rn source and assume the main origin of $^{222}$Rn under the inversion layer to be its soil flux. Hence, temporal evolution of $^{222}$Rn vertical distribution under the inversion layer of the height $H$ allows us to calculate the accumulation rate $Q$ [Bq s$^{-1}$] for its total amount below $H$, which gives an estimate for $^{222}$Rn soil flux as far as the assumptions (1 to 5) hold. In this case, the general problem of atmospheric $^{222}$Rn vertical and temporal variations reduces to the solution of a non-stationary diffusion equation:

$$\frac{\partial c}{\partial t} = \frac{\partial}{\partial z}\left(K(z)\frac{\partial c}{\partial z}\right) - \lambda c, \qquad z_0 < z < H(t), \qquad t \in [t_1, t_2] \tag{1}$$

where $c$ [Bq m$^{-3}$] is $^{222}$Rn concentration, $K$ [m$^2$ s$^{-1}$] is the height-dependent $^{222}$Rn diffusivity, $\lambda$ (= $2.08 \times 10^{-6}$ s$^{-1}$) is the radon decay constant, $z_0$ (= 4 m a.g.l.) is the time independent measurement height at which $c_0 \equiv c(z_0, t \geq t_1)$ is the known function represented by the actually measured $^{222}$Rn concentrations. The appropriate initial and boundary conditions for Eq. (1) are:

$$c(z, t_1) = c_0(t_1), \qquad (z_0 \leq z \leq H_{t=t_1}) \tag{2}$$

$$c(z_0, t) = c_0(t), \quad \left(\frac{\partial c}{\partial z}\right)_{z=H} = 0. \qquad (t_1 < t < t_2) \tag{3}$$

Thus, according to Eq. (2) at the start time $t_1$ $^{222}$Rn concentration is equal to its value measured prior to the inversion formation and assumed to be uniformly distributed with height due to active daytime vertical mixing. A simple explicit time-forward second order





ACPD
13, 14545–14579, 2013

space-centered scheme was used to solve Eqs. (1)–(3) on a 1-dimensional grid with $\Delta_z = 1$ m grid spacing between adjacent vertical levels and with 6 s time step to satisfy general stability requirements for a chosen $K(z)$ profiles. Once vertical distribution of radon is known, the total $^{222}$Rn abundance $M$ and accumulation rate $Q$ within a layer $0 \le z \le H$ at a time $t_i$ can be calculated by:

$$M(t_i) = \int_0^H c(t,z)\,\mathrm{d}z = \sum_j c(z_j, t_i)\cdot\Delta_z, \tag{4}$$

$$Q = \overline{(\mathrm{d}M/\mathrm{d}t)}^t \approx (M_{t=t_2} - M_{t=t_1})/(t_2 - t_1), \tag{5}$$

where the summation is performed over the computational cells and a horizontal bar denotes time averaging.

In the case of strong inversion the diffusion coefficient $K$ near the earth's surface is known to be very weak, yet being quite variable with $z$ depending on the vertical variations of wind velocity and stability. Following to Cohen et al. (1972) we assume in the present study a linear dependence of $K$ on $z$, with the upper-layer $K$ being independent of height and in the surface layer below 100 m being given as

$$K(z) = K(z_1)\cdot z/z_1, \qquad (z < H) \tag{6}$$

where $K(z_1)$ is some known diffusivity rate at a reference level. In our calculations the value of $H$ is set to be constant and was chosen from numerical experiments to be so high (~ 600 m) that it does not affect at any appreciable rate the final estimates of radon fluxes. We derive a plausible range for warm-season $K(z_1)$ diffusivities along the TROICA route basing on the corresponding modal values at heights 50–100 m a.g.l. from NOAA ARL Archived Meteorology database (http://ready.arl.noaa.gov/READYamet.php). We chose $K(z)$ profiles characteristic of two stability classes of ABL: $\Delta T_{100} > 4.0\,^{\circ}$C – extremely stable (G), and $\Delta T_{100} = 1.5$–$4.0\,^{\circ}$C – moderately stable





ACPD
13, 14545–14579, 2013

(F) according to the common classification of Pasquill (1961), where $\Delta T_{100}$ is a temperature change in the near-surface 100 m layer. Table 2 shows the surface temperature inversion characteristics from the TROICA dataset averaged for different seasons with the strongest positive temperature gradients observed in spring and autumn experiments (TROICA-8 and 9) owing to anticyclonic weather conditions over the most part of the route. Hence, the selected classes G and F cover completely the range of $\Delta T_{100}$ values observed during the TROICA experiments for nocturnal surface inversions. We apply

$$K(z_1) = \begin{cases} 10\,\mathrm{sm}^2\,\mathrm{s}^{-1} \text{ for class G,} \\ 100\,\mathrm{sm}^2\,\mathrm{s}^{-1} \text{ for class F.} \end{cases} \quad z_1 = 1\,\mathrm{m}, \tag{7}$$

which are also in a good agreement with the results presented in Bezuglaya (1983) for Russian regions and with the vertical diffusivity profiles given by Jacobi and Andre (1963) (their curves WNW and IWN on Fig. 1) used in the relevant studies on $^{222}$Rn distribution (Beck and Gogolak, 1979; Moses et al., 1960) as well as with the average $K$ values in a 90 m depth surface layer proposed in Hosler et al. (1983) for the F stability class. Since a particular value of the diffusivity rate has a first-order influence on the final estimates of $^{222}$Rn fluxes, two series of the calculations with $K(z_1)$ value given by Eq. (7) were carried out to assess a plausible range of radon soil fluxes for each observational episode.

# 3 Results and discussion

## 3.1 Variations of surface $^{222}$Rn concentration over Russia

### 3.1.1 $^{222}$Rn spatial distribution

Figure 2 shows the spatial distribution of original 10 min mean $^{222}$Rn concentrations and 10th, 50th and 90th percentiles calculated for 100 km parts of the route.





ACPD
13, 14545–14579, 2013

For spring and autumn data only the 50th percentile values are considered because of a limited dataset for calculations. The figure also presents the altitude a.s.l. along the Trans-Siberian Railway to demonstrate an importance of terrain elevation in the observed radon distribution. For the regional-scale representation, we divided the Russian territory along the Trans-Siberian Railway into 6 regions according to their basic geological features: ETR, European territory of Russia (Moscow–Perm), Ural (Perm–Ekaterinburg), Western Siberia (Ekaterinburg–Novosibirsk), Central Siberia (Novosibirsk–Irkutsk), Eastern Siberia (Irkutsk–Belogorsk) and the Far East (Belogorsk–Vladivostok). One can see from the figure that significant variations of radon concentrations exist in each season even within geologically uniform areas. It should be noted, however, that simple examination of the displayed time series does not provide any information about the true geographical areas of enhanced radon fluxes, since the measured surface concentrations depend strongly on vertical exchange rate driven by ABL daily variations and hence can be strongly connected to the local observation time. The marked increase in radon concentrations seen at some parts of the route is found to be controlled by a night-time accumulation effect in temperature inversion conditions, which overrides the possible influence of other contributing factors. Some appropriate statistics on spatially averaged 1 h diurnal and daytime $^{222}$Rn concentrations for each region and the inversion characteristics averaged for the Russian regions from the summer and autumn observations are shown in Tables 2 and 4, correspondingly (the spring measurements were excluded from consideration because of a lack of the data for spatial averaging). The table shows that in most cases the diurnal mean $^{222}$Rn concentrations are significantly higher for all seasons and regions than the daytime ones due to the night-time accumulation effect (discussed in detail in Sect. 3.1.2) However, there are some episodes (see Table 3) with high daytime mean radon concentrations in spring (European territory and Ural) and autumn (European territory and the Far East). Table 4 presents the inversion characteristics averaged for the Russian regions from the summer and autumn observations. Prolonged temperature inversions existed up to mid-day hours in these observational periods in the





ACPD
13, 14545–14579, 2013

regions under consideration (Tables 2 and 4) and could contribute to such high daytime radon concentrations. The limited number of the experiments performed in each season (see Table 1) does not allow us to filter out the night-time accumulation signal from the observational data completely. So, we describe here some large-scale features of spatial $^{222}$Rn distribution based on daytime statistics (listed in Table 3) rather than on diurnal means assuming the former be more representative for a background atmospheric radon levels over the continent.

According to Table 3, the highest daytime radon concentrations were observed in the Far East (12.4 and 7.3 Bq m$^{-3}$ in autumn and summer on average, respectively) and in Central Siberia (7.8 and 6.9 Bq m$^{-3}$ in autumn and summer on average, respectively). According to the summer and spring experiments, low $^{222}$Rn concentrations, 2–7 Bq m$^{-3}$, are typical for the ETR and West Siberian regions characterized by flat terrain with low absolute elevations. However, in the autumn 2005 experiment high $^{222}$Rn concentrations, up to 13 and 18 Bq m$^{-3}$ in the ETR and Western Siberia, correspondingly, were observed (see Fig. 2 and Table 3). The probable reason of this radon increase is a cumulative effect of two factors: steady anticyclonic conditions with strong and prolonged (up to 16 h) surface temperature inversions and the existence of significant regional anthropogenic sources.

On the whole, $^{222}$Rn concentrations are higher in autumn comparing to other seasons in all Russian regions (see Fig. 2 and Table 5). The factors which can determine such seasonal $^{222}$Rn variations will be discussed further in the Sects. 3.1.3 and 3.1.4.

Table 3 shows that there exists some negative correlation in near-surface radon abundances between the western (ETR – Western Siberia) and eastern (Central and Eastern Siberia) parts of the continental areas of North Eurasia. This feature was earlier observed in the seasonal variability of surface air abundances of other trace gases as well (Elansky et al., 2009) and can be most probably connected to a long-wave trough/ridge system commonly persisted over the continental areas of the North Eurasia including the periods of the TROICA experiments.





ACPD
13, 14545–14579, 2013

We compared $^{222}$Rn concentrations from the TROICA experiments with the Map of radon risk of Russia (Maximovsky et. al., 1996) compiled on the basis of the generalized analytical data on radiogeochemistry, radiometric investigation and other materials obtained from long-term researches of different Russian scientific organizations. The authors of the map divided Russian territory into geographical areas according to the degree of radon risk, as shown in Fig. 2. According to the TROICA data, radon concentrations in the areas of elevated radon risk shown on the map are commonly lower than that measured in the dangerous areas (see Table 4 and Fig. 2). The observed high $^{222}$Rn concentrations between Magdagachi and Arkhara (Fig. 2) cover both the radon dangerous area and the "radon Clarke" area (the area where $^{222}$Rn concentration is equal or below its average in the earth's crust) on the map of radon risk immediately to the west, which is likely to be due to the prevailing effect of the local observation times as discussed above. Generally, $^{222}$Rn concentrations measured in the TROICA experiments (Fig. 2) are found to be in a good agreement with the earlier studies on the radon risk areas (Maximovsky et. al., 1996) as well as spatial locations of tectonic faults, which confirms our general notion about the reliability of the obtained $^{222}$Rn dataset and its applicability to invert radon soil fluxes at a regional basis.

#### 3.1.2 Effect of the atmospheric stability on surface $^{222}$Rn concentration

In TROICA experiments, the highest $^{222}$Rn concentrations (up to 75 Bq m$^{-3}$) were commonly observed during the nights with strong and prolonged surface temperature inversions. Figure 3 shows the mean diurnal cycles of temperature inversion height and $^{222}$Rn concentration in different seasons. The surface temperature inversions existed usually from 18:00–19:00 to 06:00–08:00 LT and from 17:00 to 09:00–10:00 LT in the warm and cold seasons, correspondingly (Fig. 3a). The highest radon concentrations, up to 30–35 Bq m$^{-3}$ were observed in the early morning (04:00–06:00 LT), being a result of night-time accumulation below temperature inversion, prior to the beginning of inversion collapse and subsequent decrease in $^{222}$Rn concentration as a factor of 3





ACPD
13, 14545–14579, 2013

to 5 on average owing to convective mixing. Contrary, in the absence of temperature inversions there were no night-time near-surface radon accumulation episodes, so its mean concentration did not change significantly during the day and for all seasons was 1.5–3.5 Bq m$^{-3}$ (Fig. 3b with the caption "no inversions").

Table 5 presents diurnal and daytime mean $^{222}$Rn concentrations in different seasons according to the TROICA measurements. The measurements performed under daytime inversion conditions were excluded from the present data to suppress the strong effect of the associated radon accumulation on the derived statistics, which resulted in daily mean $^{222}$Rn concentrations being 1.5–2 times lower on average compared to the diurnal ones in all seasons. The highest diurnal and daytime mean $^{222}$Rn concentrations were observed in autumn owing to the strongest and most prolonged temperature inversions observed in this period (see Tables 2 and 4), which confirms significant influence of vertical exchange rates on surface $^{222}$Rn variations at a seasonal scale.

#### 3.1.3 Seasonal soil thawing effect on surface $^{222}$Rn concentration

Along with vertical exchange due to the turbulent mixing, the properties of the soil is the other key factor affecting $^{222}$Rn near-surface abundance. The soil covered with snow or ice accumulates $^{222}$Rn and makes for its subsequent enhanced emission into the atmosphere during the first hours after snow melting (Miklyaev and Petrova, 2007). Commonly, the diffusion equilibrium between the soil and the surface atmospheric layer is reached in several hours after which the radon flux attains its steady-state value but sometimes this process can last up to several days. Glover (2006) and Glover and Blouin (2007) note that the permafrost is a barrier to $^{222}$Rn exhalation resulting in its 80–90 % decrease in ambient air and 10–15 times increase in its abundance in the soil. Since the major part of the Trans-Siberian Railway in East Siberia goes through the permafrost area, the influence of seasonal soil thawing should be accounted for when studying seasonal aspects of the $^{222}$Rn surface flux variations.

The thawing depth was calculated in the region 52–55° N, 105–130° E at the time periods of the TROICA campaigns using the scheme of the heat and moisture transfer



ACPD
13, 14545–14579, 2013



Title Page
Abstract | Introduction
Conclusions | References
Tables | Figures
◄ | ►
Back | Close
Full Screen / Esc
Printer-friendly Version
Interactive Discussion

in the soil (Arzhanov et al., 2008) in the ECHAM5/MPI-OM model (SRES A1B scenario). The resulting effect of the thawing depth on the near-surface radon abundance is shown in Fig. 4. The model-predicted thawing depth is approximately 1.24, 1.40 and 1.85 m for the Summer TROICA-5,7,11, Summer TROICA-12, and October TROICA-9 campaigns, correspondingly. One can see from the figure, that near-surface radon concentrations increased more than 3 times (accordng to the daytime radon values) in this region from summer 1999 (TROICA-5) to summer 2008 (TROICA-12) reaching the highest value in autumn 2005 (TROICA-9), with the persistent increase in thawing depth being observed. To exclude the effect of the night-time radon accumulation events, we divided nighttime and daytime data (see Fig. 4). Yet, the impact of the thawing depth is seen distinctly for both the night and daytime $^{222}$Rn concentrations; hence, the observed increase in the seasonal thawing depth during the warm period can explain higher $^{222}$Rn concentrations in autumn comparing with other seasons.

### 3.2 Nocturnal $^{222}$Rn soil flux calculation

We use the measured $^{222}$Rn concentrations in nocturnal accumulation events to estimate associated radon surface fluxes using the numerical approach discussed in Sect. 2.3. An example of $^{222}$Rn flux calculation at the route part 1256–1076 km from Moscow 10 July 2001, 02:54–06:10 LT (TROICA-7) is presented in Fig. 6. The observed region is located in a flat area with a typical elevation from 150–200 m a.s.l. The figure shows the time series of the atmospheric temperatures at different heights a.g.l., the measured radon concentration, and the calculated total radon content varying approximately linear with time. Invoking Eq. (6), the regression slope of $M$ on $t$ gives the mean radon emission rate, which is an approximate estimate for $Q$.

In a particular nighttime accumulation event the atmospheric transport conditions within the surface inversion layer vary both with time and altitude with the resulting effect on radon accumulation rate hardly to be quantified at a rational basis taking into account the lack of observational data on the full set of parameters governing the turbulent mixing regime. In present simulations the major factor affecting the radon vertical distribution, and hence accumulation rate, is the vertical mixing rate profile controlled by the parameter $K(z_1)$. Since the exact value of the temperature gradient in a particular inversion event changes within a range of G and F stability classes, two sets of calculations were performed by setting $K(z_1)$ equal to 10 and 100 $\text{cm}^2\,\text{s}^{-1}$ according to Eq. (7) to obtain $Q$(G) and $Q$(F) values for radon accumulation rates for G and F stability classes, respectively. Accordingly, for each accumulation event $i$ we define

$$\overline{Q}_i = (Q_\text{G} + Q_\text{F})/2, \qquad \sigma_{Q,i} = |Q_\text{G} - Q_\text{F}|/2 \tag{8}$$

as the best estimates for $Q$ and an estimate error for $\overline{Q}_i$, correspondingly. The relative estimated error is commonly a few tens of percent and reaches as much as 50 % in some events. To make our estimates be representative at a regional scale, we calculate the expected means and associated errors as

$$\overline{Q}_\text{reg} = \sum_i g_i \cdot \overline{Q}_i / \sum_i g_i, \tag{9}$$

and

$$\sigma_{Q,\text{reg}} = \left(\sum_i g_i\right)^{-2}, \tag{10}$$

correspondingly, where $g_i = \sigma_{Q,i}^{-1}$, and summation by $i$ is performed over all accumulation events observed during the TROICA expeditions within a particular region defined according to Fig. 2. The calculated weighted-mean region averaged radon soil fluxes are summarized in Fig. 6 and Table 6. One can see that the derived $^{222}$Rn soil flux varies significantly over Russia, from 0.01 to 0.15 $\text{Bq}\,\text{m}^{-2}\,\text{s}^{-1}$, depending on the geological features as well as the seasons. In the mountain regions of Central and Eastern Siberia, the Far East, radon soil emissions are 1.5–3 times higher than in the plains (Table 6), with the maximum values being found in the regions with tectonic faults.

We compared $^{222}$Rn fluxes calculated from the TROICA experiments with the $^{222}$Rn flux maps derived from the data modeling. Schery and Wasiolek (1998) proposed a global $^{222}$Rn flux map based on a porous media transport theory and calibrated them with experimental $^{222}$Rn flux data from Australia and Hawaii. The map gives $^{222}$Rn flux for the Russian latitudes to be about 0.02–0.03 Bq m$^{-2}$ s$^{-1}$ but has a large unsertainty becouse of the lack of global data on soil moisture and $^{226}$Ra content. Hirao et al. (2010) improved the performance of the model complimented by the soil and $^{226}$Ra content and estimated the global $^{222}$Rn flux density distribution in the period of 1979–2007. These estimations give $^{222}$Rn flux for Russian regions to be up to 0.03 Bq m$^{-2}$ s$^{-1}$. The $^{222}$Rn flux estimations by Schery and Wasiolek (1998) and Hirao et al. (2010) are in the range of our estimations but as a rule 5–6 times lower then our ones. The Russian $^{222}$Rn flux map (http://radon.unibas.ch) generated by the scientific group from the University of Basel, Switzerland (Szegvary et al., 2007) and based on a gamma-dose rate map of Russia derived from aeroradiometric measurements (Vysokoostrovskaya et al., 1995) shows the highest radon fluxes in Central and Eastern Siberia, in the Far East that corresponds to our estimations. But according to the map, $^{222}$Rn flux varies over Russia from 0.2 to 1.2 atom cm$^{-2}$ s$^{-1}$ (from 0.004 to 0.02 Bq m$^{-2}$ s$^{-1}$) which is 3–7 times lower than the range we inferred.

Our estimations are in a good agreement with the direct $^{222}$Rn flux measurements reported for some Russian regions. According to the Perm CGMS radiation monitoring, in 2006 the mean $^{222}$Rn flux was $0.04 \pm 0.01$ Bq m$^{-2}$ s$^{-1}$ in the Perm region (http://wp.permecology.ru/report/report2006/17.html) which corresponds to $0.04 \pm 0.02$ Bq m$^{-2}$ s$^{-1}$ on average from the TROICA experiments. $^{222}$Rn soil fluxes in Krasnoyarsk city and its suburb Minusinsk reported to vary from 0.014 to 0.2 Bq m$^{-2}$ s$^{-1}$ and from 0.009 to 0.6 Bq m$^{-2}$ s$^{-1}$, correspondingly (Voevodin and Kurguz, 2012; Sobyanina et al., 2012) being 0.04 Bq m$^{-2}$ s$^{-1}$ on average. These measurements are in a good agreement with our estimations ($0.04 \pm 0.03$). Bolshakov and Seyvald (2005) measured $^{222}$Rn flux in Tomsk from September to Oktober 2004 to be from 0.02 to 0.7 Bq m$^{-2}$ s$^{-1}$. Our estimations give $^{222}$Rn flux in this region in summer months to be $0.04 \pm 0.01\,\mathrm{Bq\,m^{-2}\,s^{-1}}$. Milin et al. (1967) reported the mean $^{222}$Rn flux from summer measurements in Kirov to be about $0.02\,\mathrm{Bq\,m^{-2}\,s^{-1}}$ which is in a good agreement with our calculations ($0.02 \pm 0.01\,\mathrm{Bq\,m^{-2}\,s^{-1}}$). Miklyaev and Petrova (2006) measured $^{222}$Rn flux at different sites in Moscow and reported that $^{222}$Rn flux varies from 0.01 to $0.07\,\mathrm{Bq\,m^{-2}\,s^{-1}}$ ($0.02 \pm 0.01$ on average) in the regions with clay soils. $^{222}$Rn fluxes calculated from the observations on the mobile laboratory around Moscow (TROICA-10, 4–7 October 2006) at two observational parts in the east of the Moscow region, where the clay soils are spread, were $0.01 \pm 0.008$ and $0.02 \pm 0.007\,\mathrm{Bq\,m^{-2}\,s^{-1}}$. On the whole, $^{222}$Rn soil flux over Russia can vary from 0.01 to $0.07\,\mathrm{Bq\,m^{-2}\,s^{-1}}$ (Milin et al., 1967; Kirichenko 1970) in agreement with our calculations.

## 4 Conclusions

The most significant variations in surface radon concentrations along the Trans-Siberian Railway are caused by the diurnal change in the ABL stability. The highest $^{222}$Rn concentrations (up to $75\,\mathrm{Bq\,m^{-3}}$) were usually observed during night-time strong and prolonged temperature inversions in the mountain regions of Russia (Central and Eastern Siberia, the Far East). Due to weak vertical mixing in the stable atmosphere, $^{222}$Rn accumulates in ASL and its concentrations increased several times compared to its values during unstable atmospheric conditions. If we know the rate of $^{222}$Rn accumulation in the night-time stable ABL and the height of its mixing layer, we can estimate nocturnal radon soil flux.

The calculated nocturnal $^{222}$Rn soil flux over Russia varies from 0.01 to $0.15\,\mathrm{Bq\,m^{-2}\,s^{-1}}$, with the highest values for the mountain regions of Central Siberia and the Far East. Generally, $^{222}$Rn concentration and flux over Russia peak in autumn and bottom out in spring. We suppose that there is a contribution to high radon concentrations and fluxes in the permafrost regions in autumn by seasonal soil thawing.





ACPD
13, 14545–14579, 2013

It is possible that air advection from local anthropogenic radon sources has some effect on surface radon concentration variations in stable atmospheric conditions but such requires a detailed investigation.

$^{222}Rn$ fluxes estimated from the experiments on the mobile laboratory are in agreement with the data reported for Russian regions in literature. This information is beyond doubt of importance to investigate and document in detail the trends in fluxes of $N_2O$, $CO_2$, and $CH_4$ during the coming decades of global warming in the mid-Anthropocene (http://www.fu-berlin.de/sites/einsteinlectures/el_2008_1_crutzen/index.html).

*Acknowledgements.* The authors thank P. Crutzen, H. Paretzke, G. S. Golitsin, O. V. Lavrova, A. I. Skorokhod for their support, active participation in the organization and/or carrying out of the TROICA experiments, I. B. Belikov and R. A. Shumsky for providing the experimental data, M. M. Arzhanov for the calculation of the seasonal thawing depth under permafrost conditions in the periods of the TROICA experiments, A. N. Safronov for his help with ArcView GIS data processing. The work is supported by the Russian Basic Research Foundation (projects No. 13-05-00461, 10-05-00272) and the 4th RAS Presidium Program.

## References

Arzhanov, M. M., Eliseev, A. V., Demchenko, P. F., Mokhov, I. I., and Khon, V. Ch.: Simulation, of thermal and hydrological regimes of Siberian river watersheds under permafrost conditions from reanalysis data, Izvestiya, Atmos. Ocean. Phys., 44, 83–89, 2008.

Beck, H. and Gogolak, C.: Time-dependent calculations of the vertical distribution of $^{222}Rn$ and its decay products in the atmosphere, J. Geophys. Res., 84, 9C0385, 3139–3148, 1979.

Berezina, E. V. and Elansky, N. F.: $^{222}Rn$ concentrations in the atmospheric surface layer over continental Russia from observations in TROICA experiments, Izvestiya, Atmos. Ocean. Phys., 45, 757–769, 2009.

Bezuglaya, E. Yu.: Climate Characteristics of Species Spreading Conditions in the Atmosphere, Gidrometeoizdat, Leningrad, 326 pp., 1983.

Biraud, S., Ciais, P., Ramonet, M., Simmonds, P., Kazan, V., Monfray, P., O'Doherty, S., Spain, T., and Jennings, S.: European greenhouse gas emissions estimated from contin-





ACPD

13, 14545–14579, 2013



Title Page
Abstract | Introduction
Conclusions | References
Tables | Figures
◀| |▶
◀ ▶
Back | Close
Full Screen / Esc
Printer-friendly Version
Interactive Discussion

uous atmospheric measurements and radon-222 at Mace Head, J. Geophys. Res., 105, 1351–1366, 2000.

Bolshakov, O. S., Seyvald, N. A.: Research of daily dynamics of radon flux density from the Earth's surface, in: Problems of Geology and Mineral Resources Development, Proceedings of M.A. Usov Ninth. International Symposium, Tomsk, TPU, 595–597, 2005.

Cohen, L. D., Barr, S., Krablin, R., and Newstein, H.: Steady-state vertical turbulent diffusion of radon, J. Geophys. Res., 77, 2654–2668, 1972.

Conen, F. and Robertson, L. B.: Latitudinal distribution of Rn-222 flux from continents, Tellus B, 54, 127–133, 2002.

Corazza, M., Bergamaschi, P., Vermeulen, A. T., Aalto, T., Haszpra, L., Meinhardt, F., O'Doherty, S., Thompson, R., Moncrieff, J., Popa, E., Steinbacher, M., Jordan, A., Dlugokencky, E., Brühl, C., Krol, M., and Dentener, F.: Inverse modelling of European $N_2O$ emissions: assimilating observations from different networks, Atmos. Chem. Phys., 11, 2381–2398, doi:10.5194/acp-11-2381-2011, 2011.

Dörr, H., Kromer, B., Levin, I., Münnich, K., and Volpp, H.: $CO_2$ and radon as tracers for atmospheric transport, J. Geophys. Res., 88, 1309–1313, 1983.

Druilhet, A., Guedalia, D., Fontan, J., and Laurant, J.: Study of radon 220 emanation deduced from measurement of vertical profiles in the atmosphere, J. Geophys. Res., 77, 6508–6514, 1972.

Dueñas, C., Fernandez, M. C., Cañete, S., Carretero, J., and Liger, E.: $^{222}$Rn concentrations, natural flow rate and the radiation exposure level in the Nerja Cave, Atmos. Environ., 33, 501–510, 1999.

Elansky, N. F., Belikov, I. B., Berezina, E. V., Brenninkmeijer, C. A. M., Buklikova, N. N., Crutzen, P. J., Elansky, S. N., Elkins, J. V., Elokhov, A. S., Golitsyn, G. S., Gorchakov, G. I., Granberg, I. G., Grisenko, A. M., Holzinger, R., Hurst, D. F., Igaev, A. I., Kozlova, A. A., Kopeikin, V. M., Kuokka, S., Lavrova, O. V., Lisitsyna, L. V., Moeseenko, K. B., Oberlander, E. A., Obvintsev, Yu. I., Obvintseva, L. A., Pankratova, N. V., Postylyakov, O. V., Putz, E., Romashkin, P. A., Safronov, A. N., Shenfeld, K. P., Skorokhod, A. I., Shumsky, R. A., Tarasova, O. A., Turnbull, J. C., Vartiainen, E., Weissflog, L., and Zhernikov, K. V.: Atmospheric Composition Observations over Northern Eurasia Using the Mobile Laboratory: TROICA Experiment, edited by: Elansky, N. F., Agrospas, Moscow, Russia, 72 pp., 2009.

Gaudry, A., Polian, G., Ardouin, B., and Lambert, G.: Radon-calibrated emissions of $CO_2$ from South Africa, Tellus B, 42, 9–19, 1990.





ACPD
13, 14545–14579, 2013

Estimation of nocturnal $^{222}$Rn soil fluxes over Russia

E. V. Berezina et al.

Glover, P. W. J.: Increased domestic radon exposure caused by permafrost thawing due to global climate change, EGU General Assembly, Vienna, Austria, 2–7 April, EGU06-A-01439, 2006.

Glover, P. W. J. and Blouin, M.: Modelling increased soil radon emanation caused by instantaneous and gradual permafrost thawing due to global climate warming, EGU General Assembly, Vienna, Austria, 15–20 April, EGU2007-A-07657, 2007.

Hirao, S., Yamazawa, H., and Moriizumi, J.: Estimation of the global $^{222}$Rn flux density from the Earth's surface, Jpn. J. Health Phys., 45, 161–171, 2010.

Hirsch, A. I.: On using radon-222 and $CO_2$ to calculate regional-scale $CO_2$ fluxes, Atmos. Chem. Phys., 7, 3737–3747, doi:10.5194/acp-7-3737-2007, 2007.

Hosler, C. R.: Meteorological effects on atmospheric concentrations of Radon (Rn-222), RaB (Pb-214), and RaC (Bi-214) near the ground, Mon. Weather Rev., 94, 89–99, 1966.

Jacobi, W. and Andre, K.: The vertical distribution of radon-222, radon-220 and their decay products in the atmosphere, J. Geophys. Res., 68, 3799–3814, 1963.

Kadygrov, E. N. and Pick, D. R.: The potential for temperature retrieval from an angular scanning single-channel microwave radiometer and some comparison with in situ observations, Meteorol. Appl., 5, 393–404, 1998.

Kataoka, T., Yunoki, E., Shimizu, M., Mori, T., Tsukamoto, O., Ohashi, Y., Sahashi, K., Maitani, T., Miyashita, K., Fujikawa, Y., and Kudo, A.: Diurnal variation in radon concentration and mixing-layer depths, Bound.-Lay. Meteorol., 89, 225–250, 1998.

Kirichenko, L. V.: Radon exhalation from vast areas according to vertical distribution of its short-lived decay products, J. Geophys. Res., 75, 3639–3649, 1970.

Lee, H. N. and Larsen, R. J.: Vertical diffusion in the lower atmosphere using aircraft measurements of radon-222, J. Appl. Meteorol., 36, 1262–1270, 1997.

Levin, I., Glatzer-Mattheier, H., Marik, T., Cuntz, M., Schmidt, M., and Worthy, D. E.: Verification of German methane emission inventories and their recent changes based on atmospheric observations, J. Geophys. Res., 104, 3447–3456, 1999.

Map of natural gamma radiation doses of Russia. 1 : 10 000 000 scale, Explanatory notes, Vysokoostrovskaya, E. B., Danilov, V. S., Krasnov, A. I., Reshetov, V. V., M.- SPb.: Roscomnedra, 1996.

Map of radon risk of Russia. 1 : 10 000 000 scale, Explanatory notes, Maximovsky, V. A., Smyslov, A. A., and Kharlamov, M. G., M.-SPb. (Roscomnedra, VSEGEI, Goscomvus, SPbGGI), 1996.





ACPD
13, 14545–14579, 2013

Martz, D. E., Holleman, D. F., McCurdy, D. E., and Schiager, K.: Analysis of atmospheric concentrations of RaA, RaB and RaC by alpha spectroscopy, Health Phys., 17, 131–138, 1969.
Messager, C., Schmidt, M., Ramonet, M., Bousquet, P., Simmonds, P., Manning, A., Kazan, V., Spain, G., Jennings, S. G., and Ciais, P.: Ten years of $CO_2$, $CH_4$, CO and $N_2O$ fluxes over Western Europe inferred from atmospheric measurements at Mace Head, Ireland, Atmos. Chem. Phys. Discuss., 8, 1191–1237, doi:10.5194/acpd-8-1191-2008, 2008.
Miklyaev, P. S. and Petrova, T. B.: Mechanisms of radon flux formation from the surface of soils and approached to radon hazard evaluation in areas of residential development, ANRI, 2, 2–16, 2007.
Milin, V. B., Malakhov, S. G., Zorina, K. I., and Sisigina, T. I.: Radon Concentration and Vertical Turbulent Mixing in the Lowest Atmospheric Layer, Foreign technology div Wright-Patterson AFB, Ohio, 9 February, AD0679719, 1968.
Moriizumi, J., Nagamine, K., Iida, T., Ikebe, Y.: Estimation of areal flex of atmospheric Methane in an urban area of Nagoya, Japan, inferred from atmospheric radon-222 data, Atmos. Environ., 30, 1543–1549, 1996.
Moses, H., Stehney, A. F., and Lucas, H. F.: The effect of meteorological variables upon the vertical and temporal distribution of atmospheric radon, J. Geophya. Rm., 66, 1223–1238, 1960.
Oikawa, S., Kanno, N., Sanada, T., Ohashi, N., Uesugi, M., Sato, K., Abukawa, J., and Higuchi, H.: A nationwide survey of outdoor radon concentration in Japan, J. Environ. Radioactiv., 65, 203–213, 2003.
Pasquill, F.: The estimation of the dispersion of windborne material, Meteorol. Mag., 90, 33–49, 1961.
Prospero, J. M., Bonatti, E., Schubert, E., and Carlson, T. N.: Dust in the Caribbean atmosphere traced to an African dust storm, Earth Planet. Sc. Lett., 9, 287–293, 1970.
Rasch, P. J., Feichter, J., Law, K., Mahowald, N., Penner, J., Benkovitz, C., Genthon, C., Giannakopoulos, C., Kasibhatla, P., Koch, D., Levy, H., Maki, T., Prather, M., Roberts, D. L., Roelofs, G. J., Stevenson, D., Stockwell, Z., Taguchi, S., Kritz, M., Chipperfield, M., Baldocchi, D., McMurry, P., Barrie, L., Balkanski, Y., Chatfield, R., Kjellstrom, E., Lawrence, M., Lee, H. N., Lelieveld, J., Noone, K. J., Seinfeld, J., Stenchikov, G., Schwartz, S., Walcek, C., and Williamson, D. L.: A comparison of scavenging and deposition processes in global models: results from the WCRP Cambridge Workshop of 1995, Tellus B, 52, 1025–1056, 2000.





ACPD
13, 14545–14579, 2013

Schery, S. D. and Wasiolek, M. A.: Modeling radon flux from the earth's surface, in: Radon and Thoron in the Human Environment, edited by: Katase, A. and Shimo, S., World Scientific, Singapore, 207–217, 2008.

Schmidt, M., Graul, R., Sartorius, H., and Levin, I.: Carbon dioxide and methane in continental Europe: a climatology, and 222 radon-based emission estimates, Tellus, 48, 457–473, 1996.

Servant, J.: Temporal and spatial variations of the concentration of the short-lived decay products of radon in the lower atmosphere, Tellus, 18, 663–670, 1966.

Sobyanina, E. V., Kovalenko, V. V., Maltsev, U. M., and Chechetkin, V. A.: Radon at the perspective development territory of the Severni microraion in Minusinsk, in: Proceedings of the International Scientific Conference "Radioecology of the XXI century", Krasnoyarsk, 14–16 May 2012, SFU, 165–175, 2012.

Somashekarappa, H. M., Narayana, Y., Radhakrishna, A. P., Siddappa, K., Joshi, V. B., Kholekar, R. V., and Bhagwat, A. M.: Atmospheric radon levels and its emanation rate in the environment of Kaiga, Radiat. Meas., 26, 35–41, 1996.

Stockburger, H. and Sittkus, A.: Unmittelbare Messung der naturlichen Radioaktivitat der atmospharischen Luft, Z. Naturforsch., 21a, 1128–1132, 1966.

Szegvary, T., Leuenberger, M. C., and Conen, F.: Predicting terrestrial $^{222}$Rn flux using gamma dose rate as a proxy, Atmos. Chem. Phys., 7, 2789–2795, doi:10.5194/acp-7-2789-2007, 2007.

Szegvary, T., Conen, F., and Ciais, P.: European $^{222}$Rn inventory for applied atmospheric studies, Atmos. Environ., 43, 1536–1539, 2009.

Tarasov, I. V.: Cement concretes and mortars with low natural radioactivity and radon permeability, MS thesis, Sib. Federal. Univ., Krasnoyarsk, 21 pp., 2008.

Taguchi, S., Law, R. M., Rödenbeck, C., Patra, P. K., Maksyutov, S., Zahorowski, W., Sartorius, H., and Levin, I.: TransCom continuous experiment: comparison of $^{222}$Rn transport at hourly time scales at three stations in Germany, Atmos. Chem. Phys., 11, 10071–10084, doi:10.5194/acp-11-10071-2011, 2011.

Turekian, K. K., Nozaki, Y., and Benninger, L. K.: The flux of radon and thoron from Australian Geochemistry of atmospheric radon and radon products, Annu. Rev. Earth Pl. Sc., 5, 227–255, 1977.

Voevodin, V. A. and Kurguz, S. A.: Radon flux density variation from the soil in the measurement site of Krasnoyarsk, in: Proceedings of the International Scientific Conference "Radioecology of the XXI century", Krasnoyarsk, 14–16 May 2012, SFU, 108–114, 2012.

Wilkniss, P. E., Larson, R. E., Bressan, P. J., and Steranka, J.: Atmospheric radon and continental dust near the automatic and their correlation with air mass trajectories, J. Appl. Meteorol., 13, 512–520, 1974.
Yakovleva, V. C.: The radon flux density from the Earth's surface as an indicator of a seismic activity, in: Proceedings of 7th International Conference on Gas Geochemistry, Freiberg, Germany, 22–26 September 2003, 28–30, 2003.
Yver, C., Schmidt, M., Bousquet, P., Zahorowski, W., and Ramonet, M.: Estimation of the molecular hydrogen soil uptake and traffic emissions at a suburban site near Paris through hydrogen, carbon monoxide, and radon-222 semicontinuous measurements, J. Geophys. Res., 114, D18304, doi:10.1029/2009JD012122, 2009.





ACPD
13, 14545–14579, 2013

**Table 1.** TROICA experiments: dates and routes.

| Experiment | Season | Time period | Route |
|---|---|---|---|
| TROICA-5 | summer | 26 Jun 99–2 Jul 99 | N. Novgorod–Khabarovsk |
| | | 3 Jul 99–13 Jul 99 | Khabarovsk–Moscow |
| TROICA-7 | summer | 27 Jun 01–3 Jul 01 | Moscow–Khabarovsk |
| | | 4 Jul 01–10 Jul 01 | Khabarovsk–Moscow |
| TROICA-8 | spring | 19 Mar 04–25 Mar 04 | N. Novgorod–Khabarovsk |
| | | 26 Mar 04–1 Apr 04 | Khabarovsk–Moscow |
| TROICA-9 | autumn | 4 Oct 05–10 Oct 05 | Moscow–Vladivostok |
| | | 11 Oct 05–18 Oct 05 | Vladivostok–Moscow |
| TROICA-11 | summer | 22 Jul 07–29 Jul 07 | Moscow–Vladivostok |
| | | 30 Jul 07–5 Aug 07 | Vladivostok–Moscow |
| TROICA-12 | summer | 21 Jul 08–28 Jul 08 | Moscow–Vladivostok |
| | | 29 Jul 08–4 Aug 08 | Vladivostok–Moscow |





ACPD
13, 14545–14579, 2013



Title Page
Abstract | Introduction
Conclusions | References
Tables | Figures
◀| |▶
◀ ▶
Back | Close
Full Screen / Esc
Printer-friendly Version
Interactive Discussion

**Table 2.** Surface temperature inversion characteristics averaged in different seasons.

| | | Spring (TROICA-8) | Summer (TROICA-5,7,11,12) | Autumn (TROICA-9) |
|---|---|---|---|---|
| Inversion depth, m | average (± standard deviation) | 220 ± 145 | 210 ± 119 | 198 ± 101 |
| | minimum | 50 | 50 | 50 |
| | maximum | 500 | 600 | 600 |
| Inversion intensity ($\Delta T = T_{max} - T_{4m}$), °C | average (± standard deviation) | 4.5 ± 3.7 | 2.9 ± 2.3 | 5.1 ± 3.4 |
| | minimum | 0.2 | 0.2 | 0.2 |
| | maximum | 16.9 | 13.0 | 14.9 |
| Inversion duration, min | average (± standard deviation) | 300 ± 210 | 245 ± 170 | 365 ± 300 |
| | minimum | 45 | 40 | 60 |
| | maximum | 860 | 710 | 990 |
| Temperature gradient, °C/100 m | average (± standard deviation) | 1.9 ± 0.9 | 1.3 ± 0.6 | 2.5 ± 1.3 |
| | minimum | 0.2 | 0.2 | 0.2 |
| | maximum | 6.6 | 10.7 | 8.9 |

**Table 3.** Statistics on spatially averaged 1 h diurnal and daytime $^{222}Rn$ concentrations for different Russian regions in different seasons (in $Bq\,m^{-3}$). The numbers of the regions: I – Moscow–Perm (0–1380 km from Moscow); II – Perm–Ekaterinburg (1380–1904 km from Moscow); III – Ekaterinburg–Novosibirsk (1904–3283 km from Moscow); IV – Novosibirsk–Irkutsk (3283–5136 km from Moscow); V – Irkutsk–Belogorsk (5136–7818 km from Moscow); VI – Belogorsk–Vladivostok (7818–9242 km from Moscow).

| No. | Region | Diurnal | | Daytime | | | |
|---|---|---|---|---|---|---|---|
| | | mean | st.dev | mean | st.dev | min | max |
| | | | **Spring** | | | | |
| I | European territory | 2.0 | 0.9 | 1.9 | 1.3 | 0.4 | 3.9 |
| II | Ural | 4.9 | 2.7 | 5.0 | 3.9 | 2.6 | 14.3 |
| III | Western Siberia | 6.3 | 2.5 | 5.3 | 1.9 | 3.2 | 8.8 |
| IV | Central Siberia | 6.7 | 4.3 | 6.0 | 4.3 | 1.9 | 25.5 |
| V | Eastern Siberia | 8.0 | 6.5 | 4.4 | 3.8 | 0.3 | 16.9 |
| VI | The Far East | 17.6 | 14.8 | 7.0 | 1.7 | 4.5 | 10.5 |
| | | | **Summer** | | | | |
| I | European territory | 4.0 | 4.5 | 2.1 | 3.5 | 0.1 | 4.0 |
| II | Ural | 6.9 | 7.1 | 4.7 | 1.1 | 0.5 | 6.9 |
| III | Western Siberia | 3.7 | 3.3 | 2.9 | 2.6 | 0.6 | 3.7 |
| IV | Central Siberia | 9.5 | 8.5 | 6.8 | 5.2 | 1.0 | 9.5 |
| V | Eastern Siberia | 7.5 | 6.6 | 4.6 | 4.1 | 0.3 | 7.5 |
| VI | The Far East | 8.8 | 7.0 | 7.3 | 5.8 | 0.4 | 8.8 |
| | | | **Autumn** | | | | |
| I | European territory | 12.8 | 7.0 | 13.3 | 6.4 | 7.7 | 12.8 |
| II | Ural | 22.6 | 13.4 | 7.0 | 2.2 | 4.6 | 22.6 |
| III | Western Siberia | 22.3 | 10.9 | 17.9 | 10.6 | 6.9 | 22.3 |
| IV | Central Siberia | 11.3 | 10.2 | 7.8 | 6.6 | 0.6 | 11.3 |
| V | Eastern Siberia | 9.6 | 10.2 | 6.3 | 6.3 | 1.0 | 9.6 |
| VI | The Far East | 12.4 | 7.2 | 12.4 | 7.0 | 6.7 | 12.4 |





ACPD
13, 14545–14579, 2013

**Table 4.** Surface temperature inversion characteristics averaged for the Russian regions from the summer and autumn experiments. The numbers of the regions: I – Moscow–Perm (0–1380 km from Moscow); II – Perm–Ekaterinburg (1380–1904 km from Moscow); III – Ekaterinburg–Novosibirsk (1904–3283 km from Moscow); IV – Novosibirsk–Irkutsk (3283–5136 km from Moscow); V – Irkutsk–Belogorsk (5136–7818 km from Moscow); VI – Belogorsk–Vladivostok (7818–9242 km from Moscow).

| No. | Region | Inversion depth, m | | | Inversion intensity ($\Delta T = T_{max} - T_{4\,m}$), °C | | | Inversion duration, min | | |
|---|---|---|---|---|---|---|---|---|---|---|
| | | Average (± standard deviation) | minimum | maximum | Average (± standard deviation) | minimum | maximum | Average (± standard deviation) | minimum | maximum |
| | | | | | Summer | | | | | |
| I | European territory | 220 ± 120 | 50 | 600 | 2.7 ± 1.9 | 0.2 | 11.2 | 265 ± 150 | 71 | 500 |
| II | Ural | 150 ± 80 | 50 | 350 | 1.9 ± 1.3 | 0.2 | 5.6 | 160 ± 90 | 71 | 320 |
| III | Western Siberia | 200 ± 90 | 50 | 500 | 2.9 ± 1.9 | 0.2 | 9.4 | 275 ± 105 | 125 | 382 |
| IV | Central Siberia | 225 ± 130 | 50 | 600 | 3.3 ± 2.7 | 0.2 | 11.9 | 225 ± 170 | 55 | 608 |
| V | Eastern Siberia | 200 ± 130 | 50 | 600 | 2.7 ± 2.2 | 0.2 | 14.5 | 200 ± 170 | 40 | 672 |
| VI | The Far East | 220 ± 115 | 50 | 600 | 3.1 ± 2.4 | 0.2 | 13.0 | 385 ± 215 | 105 | 711 |
| | | | | | Autumn | | | | | |
| I | European territory | 128 ± 91 | 50 | 350 | 1.8 ± 1.5 | 0.2 | 6.7 | 291 ± 320 | 100 | 771 |
| II | Ural | 215 ± 89 | 50 | 350 | 4.8 ± 2.2 | 0.2 | 10.3 | – | – | 465 |
| III | Western Siberia | 265 ± 92 | 50 | 600 | 8.0 ± 3.1 | 0.2 | 14.9 | 435 ± 351 | 100 | 800 |
| IV | Central Siberia | 179 ± 91 | 50 | 350 | 4.7 ± 3.0 | 0.2 | 13.8 | 375 ± 382 | 105 | 645 |
| V | Eastern Siberia | 225 ± 114 | 50 | 600 | 5.7 ± 3.3 | 0.2 | 16.0 | 312 ± 331 | 60 | 991 |
| VI | The Far East | 185 ± 82 | 50 | 350 | 4.1 ± 2.1 | 0.2 | 13.6 | 458 ± 341 | 70 | 861 |





ACPD
13, 14545–14579, 2013

**Table 5.** Seasonal variations of diurnal and daytime (no temperature inversions) mean $^{222}$Rn concentrations.

| | | Average (± standard deviation) | Mode | Median | Maximum | Minimum | Lower quartile (25 %) | Upper quartile (75 %) |
|---|---|---|---|---|---|---|---|---|
| Summer | diurnal | 7.2 ± 7.8 | 3.1 | 4.8 | 70.7 | < 0.1 | 2.3 | 9.3 |
| | daytime | 4.5 ± 4.1 | 3.0 | 3.2 | 21.2 | < 0.1 | 1.7 | 6.2 |
| Autumn | diurnal | 12.6 ± 10.9 | 5.2 | 9.3 | 49.4 | 0.2 | 4.2 | 17.5 |
| | daytime | 6.1 ± 4.7 | 2.2 | 5.1 | 29.6 | 0.2 | 2.2 | 8.9 |
| Spring | diurnal | 6.7 ± 6.7 | 3.6 | 4.7 | 74.8 | 0.2 | 3.0 | 7.8 |
| | daytime | 3.7 ± 2.1 | 3.6 | 3.3 | 13.4 | 0.3 | 2.3 | 4.6 |



ACPD
13, 14545–14579, 2013

Estimation of nocturnal $^{222}$Rn soil fluxes over Russia

E. V. Berezina et al.

**Table 6.** Weighted mean $^{222}Rn$ fluxes (calculated using the maximum-likelihood method) in Russian regions in different seasons. The numbers of the regions (km from Moscow): I – Moscow–Perm (0–1380 km); II – Perm–Ekaterinburg (1380–1904 km); III – Ekaterinburg–Novosibirsk (1904–3283 km); IV – Novosibirsk–Irkutsk (3283–5136 km); V – Irkutsk–Belogorsk (5136–7818 km); VI – Belogorsk–Vladivostok (7818–9242 km).

| No. | Region | $^{222}Rn$ flux (weighted mean error), $Bq\,m^{-2}\,s^{-1}$ | N (number of 10 min data points) |
|---|---|---|---|
| | | **Spring** | |
| I | European territory | – | – |
| II | Ural | 0.05 (0.04) | 26 |
| III | Western Siberia | 0.03 (0.02) | 17 |
| IV | Central Siberia | 0.07 (0.04) | 26 |
| V | Eastern Siberia | 0.06 (0.03) | 28 |
| VI | The Far East | 0.06 (0.04) | 26 |
| | | **Summer** | |
| I | European territory | 0.03 (0.01) | 101 |
| II | Ural | 0.05 (0.02) | 19 |
| III | Western Siberia | 0.04 (0.01) | 154 |
| IV | Central Siberia | 0.05 (0.01) | 87 |
| V | Eastern Siberia | 0.06 (0.01) | 193 |
| VI | The Far East | 0.06 (0.02) | 58 |
| | | **Autumn** | |
| I | European territory | 0.06 (0.03) | 27 |
| II | Ural | 0.09 (0.05) | 52 |
| III | Western Siberia | 0.09 (0.05) | 22 |
| IV | Central Siberia | 0.04 (0.02) | 80 |
| V | Eastern Siberia | 0.04 (0.02) | 5 |
| VI | The Far East | 0.07 (0.03) | 85 |





ACPD
13, 14545–14579, 2013

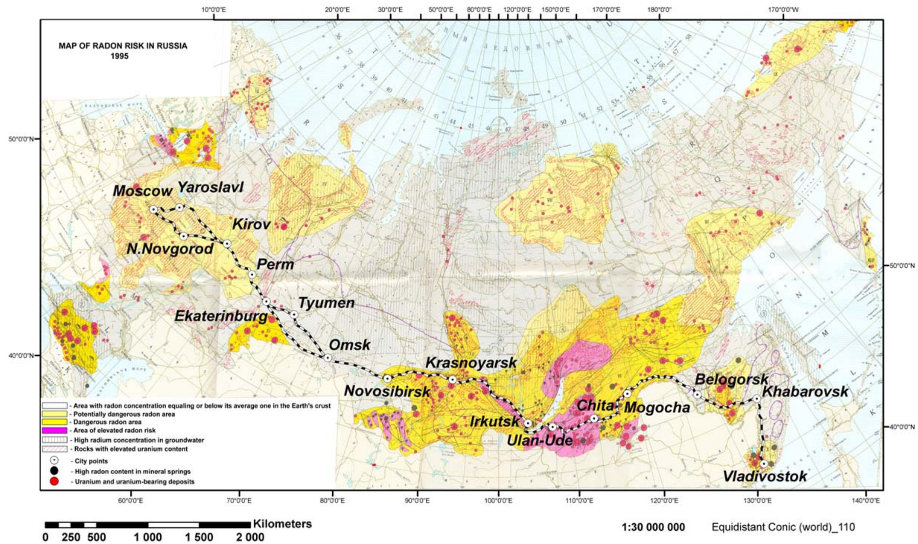


**Fig. 1.** Map of radon risk of Russia and the TROICA experiments route along the Trans-Siberian Railway from Moscow to Vladivostok.

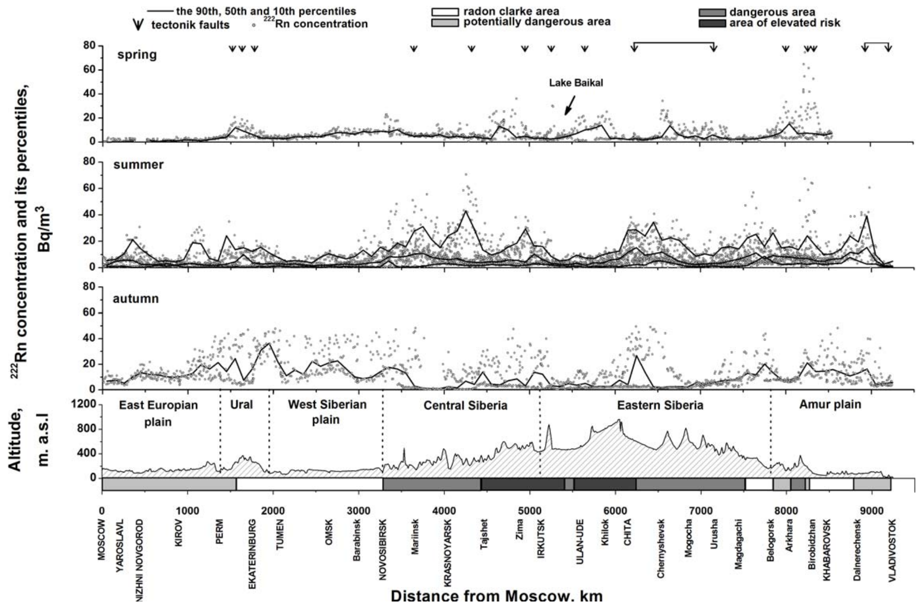


**Fig. 2.** Spatial distribution of surface $^{222}$Rn concentration (10 min average values) and altitude a.s.l. from Moscow to Vladivostok in TROICA experiments. The radon risk areas corresponding to the Map of radon risk of Russia are presented as colored rectangles. Percentiles are presented for 10 min radon values for each 100 km route part (only the 50th percentile values are presented for spring and autumn data because of a limited dataset for calculations).





ACPD
13, 14545–14579, 2013

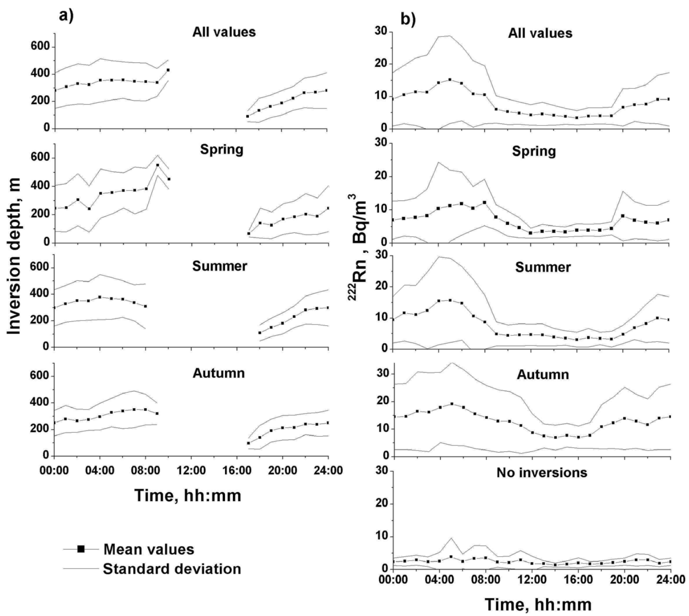


**Fig. 3.** The mean diurnal cycles of temperature inversion top **(a)** and $^{222}$Rn concentration **(b)** from TROICA experiments.





ACPD
13, 14545–14579, 2013

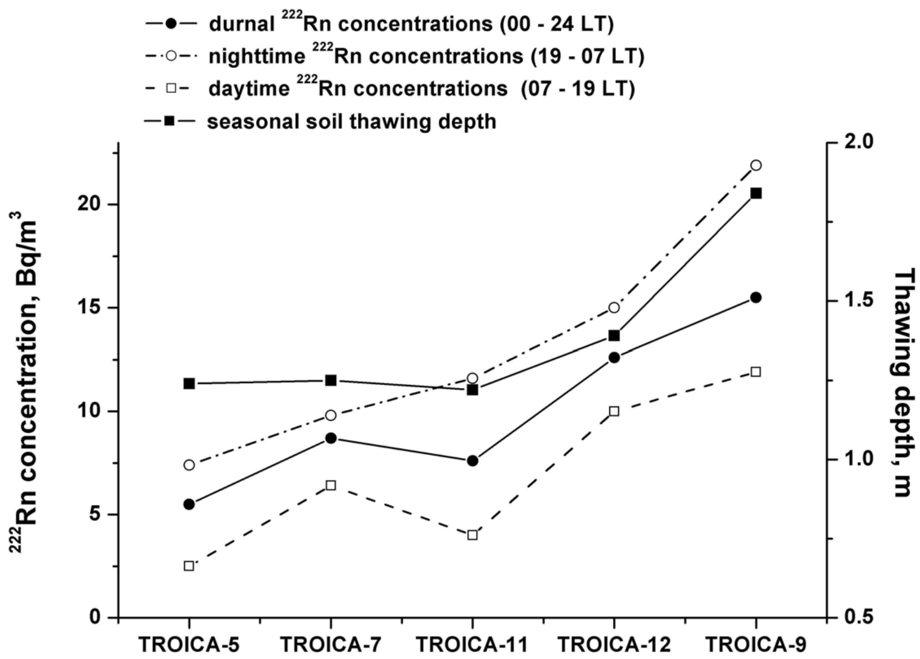


**Fig. 4.** Mean $^{222}$Rn concentrations obtained from the TROICA data and the soil thawing depth calculated for the period of the experiments in the region 52–55° N, 105–130° E using ECHAM5/MPI-OM model (SRES A1B scenario).





ACPD
13, 14545–14579, 2013

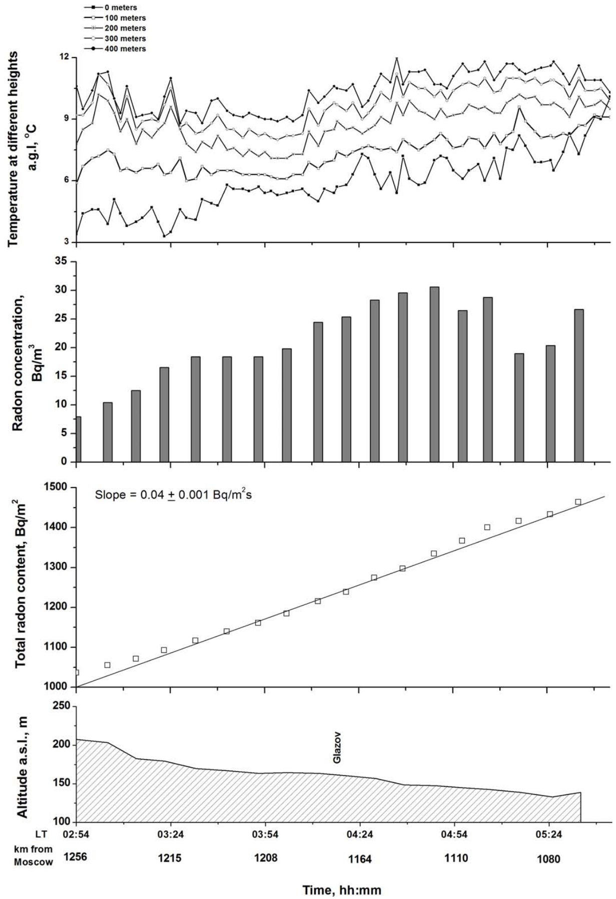


**Fig. 5.** Nocturnal $^{222}$Rn flux calculation in stable atmospheric conditions at the route part 1256–1076 km from Vladivostok to Moscow (the East European region) 10 July 2001, 02:54–06:10 LT (the TROICA-7 experiment). Slope – $^{222}$Rn flux in this region. Glazov – is the largest locality on the presented route part.





ACPD
13, 14545–14579, 2013

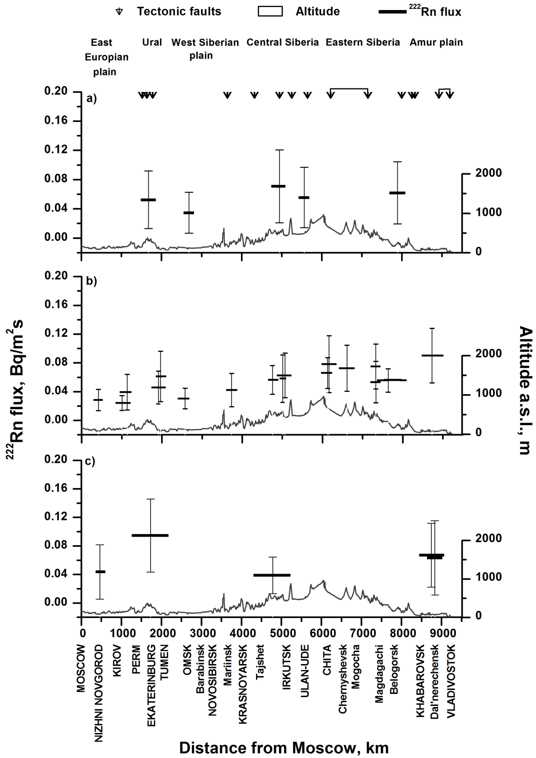


**Fig. 6.** $^{222}$Rn soil fluxes over Russia calculated from the spring **(a)**, summer **(b)** and autumn **(c)** experiments. The length of each rectangle corresponds to the route part (in km) for which $^{222}$Rn flux was estimated. The joined arrows indicate the strong faults crossing the route.





ACPD
13, 14545–14579, 2013

Estimation of nocturnal $^{222}$Rn soil fluxes over Russia

E. V. Berezina et al.